Catalytic combustion of methane over Pt and PdO-supported CeO$_2$–ZrO$_2$–Bi$_2$O$_3$/γ-Al$_2$O$_3$ catalysts

Keisuke Yasuda · Toshiyuki Masui ·
Takahiro Miyamoto · Nobuhito Imanaka

Abstract Catalytic combustion of methane was investigated on Pt and PdO-supported CeO$_2$–ZrO$_2$–Bi$_2$O$_3$/γ-Al$_2$O$_3$ catalysts prepared by a wet impregnation method in the presence of polyvinylpyrrolidone. The catalysts were characterized by X-ray fluorescence analysis, X-ray powder diffraction, X-ray photoelectron spectra, transmission electron microscopy, and BET specific surface area measurements. The Pt/CeO$_2$–ZrO$_2$–Bi$_2$O$_3$/γ-Al$_2$O$_3$ and PdO/CeO$_2$–ZrO$_2$–Bi$_2$O$_3$/γ-Al$_2$O$_3$ catalysts were selective for the total oxidation of methane into carbon dioxide and steam, and no by-products such as HCHO, CO, and H$_2$ were obtained. The catalytic activities of the PdO/CeO$_2$–ZrO$_2$–Bi$_2$O$_3$/γ-Al$_2$O$_3$ catalysts were relatively higher than those of the Pt-supported catalysts, due to the facile re-oxidation of metallic Pd into PdO based on lattice oxygen supplied from the CeO$_2$–ZrO$_2$–Bi$_2$O$_3$ bulk. A decrease in the calcination temperature during the preparation process was found to be effective in enhancing the specific surface area of the catalysts, whereby particle agglomeration was inhibited. Optimization of the PdO amount and calcination temperature enabled complete oxidation of methane at temperatures as low as 320 °C on the 11.6 wt% PdO/CeO$_2$–ZrO$_2$–Bi$_2$O$_3$/γ-Al$_2$O$_3$ catalyst prepared at 400 °C.

K. Yasuda · T. Masui · T. Miyamoto · N. Imanaka (✉)
Department of Applied Chemistry, Faculty of Engineering,
Osaka University, 2-1 Yamadaoka, Suita, Osaka 565-0871,
Japan
e-mail: imanaka@chem.eng.osaka-u.ac.jp

K. Yasuda
Japan Society for the Promotion of Science, 1-8 Chiyoda-ku,
Tokyo 102-8472, Japan

Introduction

Natural gas consists primarily of methane (CH$_4$) and is an important fuel resource. It has been used as an energy source for lean-burn natural gas vehicles (NGVs) and natural gas-fuelled gas turbines. NGV engines have an environmental advantage due to relatively lower emissions of nitrogen oxides (NO$_x$) and particulate matters compared to diesel and gasoline engines [1]. However, the major disadvantage associated with CH$_4$ utilization is not only unburned CH$_4$ emissions from NGVs, but also NO$_x$ emissions from gas turbines produced by high-temperature combustion of CH$_4$ [2]. In particular, CH$_4$ is a highly potent greenhouse gas, and its greenhouse effect is approximately 20 times higher than that of CO$_2$. Therefore, it is important to reduce CH$_4$ emissions into the atmosphere as much as possible. One of the effective abatement methods of CH$_4$ emission is the employment of catalytic exhaust converters, in which CH$_4$ elimination is achieved by catalytic oxidation at lower temperatures.

However, CH$_4$ is probably the most difficult of all the paraffins to be oxidized completely over a catalyst, because CH$_4$ oxidation requires much higher temperatures than other alkanes. Although it has been reported that CH$_4$ can be catalytically converted into carbon dioxide and steam over noble metal [3–8] and metal oxide catalysts [4, 9–13], the former catalysts, such as Pt- and PdO-based catalysts, usually exhibit higher hydrocarbon combustion activities at low temperatures. In particular, PdO-based catalysts exhibit considerably high activity for the catalytic combustion of CH$_4$. In the case of CH$_4$ combustion over the noble metal catalysts, the chemisorption of CH$_4$ molecules on noble metals is dissociative, and adsorbed methyl or methylene radicals are produced by C–H bond activation [14]. The subsequent reaction of these radicals with adsorbed oxygen

causes either direct oxidation to CO_2 and H_2O or the formation of chemisorbed formaldehyde via methoxide, methyl peroxide, or methylene oxide intermediates [15]. When the reaction proceeds by the dissociation of adsorbed formaldehyde, there are three reaction paths; desorption as HCHO, dissociation and desorption as CO and H_2, and reaction with adsorbed oxygen to produce CO_2 and H_2O via dissociation into the adsorbed CO and H atoms [16, 17]. The reaction path is dependent on the composition of the reactant gas mixture.

The rate-determining step in CH_4 oxidation over noble metal catalysts is the activation of the C–H bond for chemical bond breaking. However, it is difficult for oxygen molecules adsorbed on noble metals from the gas phase to readily activate the almost non-polar C–H bonds in CH_4 [18]. Accordingly, it is necessary to supply reactive oxygen not only to the surface, but also from the bulk, to accomplish the complete oxidation of CH_4 at the lowest possible temperatures.

In our previous studies, we found that a CeO_2–ZrO_2–Bi_2O_3 solid can exhibit excellent oxygen storage and release properties compared with the conventional CeO_2–ZrO_2 solid [19–21]. Furthermore, we demonstrated that the $Ce_{0.64}Zr_{0.16}Bi_{0.20}O_{1.90}/\gamma$-$Al_2O_3$ solid, in which $Ce_{0.64}Zr_{0.16}Bi_{0.20}O_{1.90}$ is supported on a high-surface area γ-Al_2O_3 support, has remarkable low-temperature reduction behavior below 100 °C [22, 23]. In order to develop novel catalysts that are able to completely oxidize hydrocarbons, including volatile organic compounds (VOCs) at moderate temperatures, $Pt/Ce_{0.64}Zr_{0.16}Bi_{0.20}O_{1.90}/\gamma$-$Al_2O_3$ ($Pt/CZB/Al_2O_3$) catalysts were prepared. Platinum nanoparticles were finely dispersed on the surface of the $Ce_{0.64}Zr_{0.16}Bi_{0.20}O_{1.90}/\gamma$-$Al_2O_3$ catalysts, and complete oxidation of ethylene and toluene was realized at temperatures as low as 65 [24, 25] and 120 °C [26], respectively. The addition of polyvinylpyrrolidone (PVP) as a dispersing agent in the preparation process was extremely effective to enhance the specific surface area of the catalysts and modify their pore volume and particle size, whereby the temperatures for complete oxidation of these VOCs were considerably lowered [26, 27].

In these studies, it was elucidated that the $Pt/CZB/Al_2O_3$ catalyst is significantly active for oxidation of unsaturated (ethylene) and aromatic (toluene) hydrocarbons. Therefore, in this study, $Pt/CZB/Al_2O_3$ catalysts prepared by a wet impregnation method in the presence of PVP were employed as combustion catalysts of a typical saturated hydrocarbon (methane), in addition to $PdO/Ce_{0.64}Zr_{0.16}Bi_{0.20}O_{1.90}/\gamma$-$Al_2O_3$ ($PdO/CZB/Al_2O_3$) catalysts, and their catalytic activities were investigated.

Experimental procedure

The $Ce_{0.64}Zr_{0.16}Bi_{0.20}O_{1.90}/\gamma$-$Al_2O_3$ support was prepared by a wet impregnation method in the presence of PVP K25. A small amount (5.25 times the total molar amount of cations) of PVP (mean molecular weight 35,000, mean degree of polymerization 315) was dissolved in a mixture of γ-Al_2O_3 powder (DK Fine, AA-300), aqueous solutions of $Ce(NO_3)_3$, $ZrO(NO_3)_2$, and $Bi(NO_3)_3$, and deionized water (20 mL) as solvent. The $Ce_{0.64}Zr_{0.16}Bi_{0.20}O_{1.90}$ content was adjusted to be 16 wt% of the total support to give the optimum oxygen release ability [22–26]. After the mixture was stirred at 80 °C for 6 h, the solvent was vaporized at 180 °C on an agitator with a heater, and the resulting powder was dried at 80 °C for 12 h. The sample was heated at 350 °C for 1 h to remove PVP and then calcined at 400, 500, and 600 °C for 1 h under atmospheric pressure.

The catalysts were prepared by impregnation of $Pt(NO_2)_2(NH_3)_2$ (Sigma-Aldrich) and $Pd(NO_2)_2(NH_3)_2$ (Tanaka Precious Metals) solutions into the $Ce_{0.64}Zr_{0.16}Bi_{0.20}O_{1.90}/\gamma$-$Al_2O_3$ support. After impregnation, the catalysts were dried at 80 °C for 12 h, and then calcined at 400, 500, and 600 °C for 4 h in dry synthetic air (N_2:O_2 = 79:21). The Pt and Pd loadings were adjusted in the range of 5–15 wt%.

X-ray fluorescence analysis (XRF; Rigaku ZSX100e) was used to identify the composition of the catalysts. X-ray powder diffraction (XRD; Rigaku MultiFlex) patterns were obtained with monochromatic Cu Kα radiation (40 kV, 50 mA) in the 2θ range of 10°–70°. Brunauer–Emmett–Teller (BET) specific surface area was measured using nitrogen adsorption at -196 °C (Micromeritics Tristar 3000). Transmission electron microscopy (TEM; Hitachi H-9000) was performed using an accelerating voltage of 300 kV. X-ray photoelectron spectroscopy (XPS; ULVAC 5500MT) was carried out at room temperature using Mg Kα radiation (1253.6 eV). The effect of charging on the binding energies was corrected with respect to the C 1s peak at 284.6 eV. Pellet samples of 5 mm diameter were prepared from powders and placed into an ultrahigh vacuum chamber at 10^{-7} Pa for the XPS analysis.

The CH_4 oxidation activity was tested in a conventional fixed-bed flow reactor consisting of a 10-mm diameter quartz glass tube with a feed gas mixture of CH_4 (1.0 vol%) and air (balance) at a rate of 67 mL min^{-1} over 0.2 g of catalyst, where the space velocity was 20,000 h^{-1}. The catalysts were pre-treated at 200 °C for 2 h in a flow of Ar (20 mL min^{-1}) before the catalytic activity tests to remove water molecules adsorbed on the surface of the catalyst. The catalytic activity was evaluated in terms of CH_4 conversion. The gas composition after the reaction was analyzed using a gas chromatograph with a thermal conductivity detector (TCD; Shimadzu GC-8AIT).

Results and discussion

Figure 1 shows XRD patterns of the Pt (5.3–15.2 wt%)/CZB (16 wt%)/Al_2O_3 and the PdO (5.8–16.8 wt%)/CZB (16 wt%)/Al_2O_3 catalysts. The calcination temperature of the catalysts was 500 °C. The XRD patterns of the Pt/CZB/Al_2O_3 and PdO/CZB/Al_2O_3 catalysts were consistent with those of the cubic fluorite structure and Al_2O_3, and no crystalline impurities were observed. Furthermore, in the case of the Pt/CZB/Al_2O_3 catalysts, a peak assigned to metallic platinum was observed at $2\theta = 40°$. However, for the PdO/CZB/Al_2O_3 catalysts, the palladium particles were dispersed in the oxidized state (PdO), and no metallic palladium was observed. The composition and BET
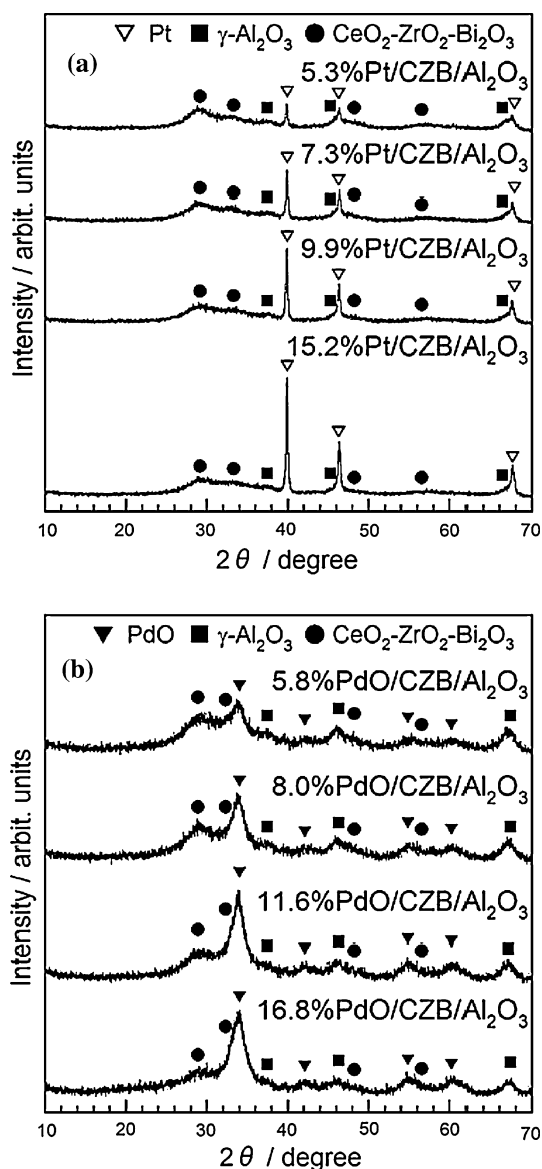
specific surface area of the catalysts prepared at 500 °C are summarized in Table 1. Using XRF analysis, the compositions of the samples were shown to be in agreement with their theoretical values within the experimental errors.

The BET specific surface area of the Pt or PdO-supported catalysts was smaller than that of the CZB (16 wt%)/Al_2O_3 support, and it decreased with an increase in the amount of Pt and PdO, which suggests that a portion of the Pt and PdO particles are supported in the pores of the CZB/Al_2O_3 support.
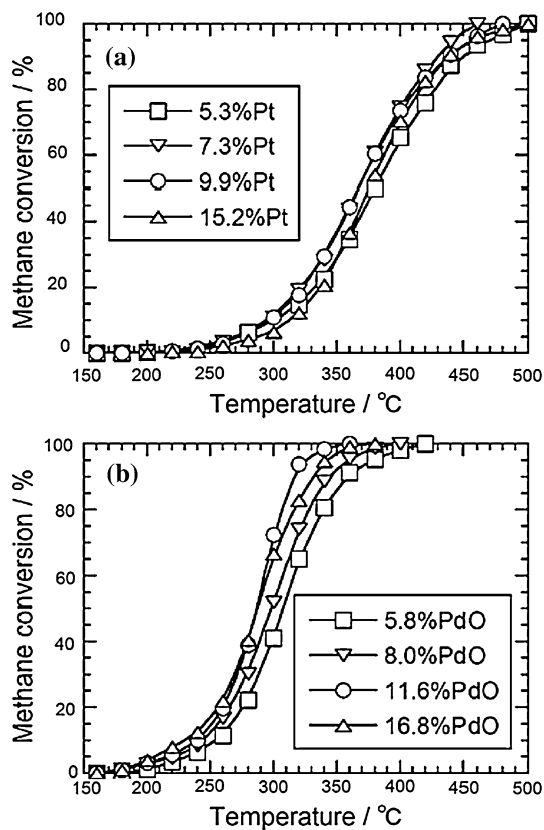
Figure 2 presents the temperature dependence of CH_4 oxidation on the Pt (5.3–15.2 wt%)/CZB/Al_2O_3 and PdO (5.8–16.8 wt%)/CZB/Al_2O_3 catalysts prepared at 500 °C. CH_4 was completely oxidized into CO_2 and steam, and no HCHO, CO, or H_2 were detected as by-products by gas chromatography mass spectrometry: no side reactions such as imperfect combustion and partial oxidation were confirmed. Among the catalysts, the highest activity was obtained for the 11.6 wt% PdO/15 wt% $Ce_{0.62}Zr_{0.17}Bi_{0.21}$ $O_{1.895}$/γ-Al_2O_3 catalyst, over which the total oxidation of CH_4 was realized at temperatures as low as 360 °C. Although the 7.3 wt% Pt/15 wt% $Ce_{0.64}Zr_{0.16}Bi_{0.20}O_{1.90}$/$\gamma$-$Al_2O_3$ catalyst was the most active for CH_4 oxidation among the Pt-supported catalysts, its catalytic activity was inferior to those of the PdO-supported catalysts, and complete oxidation of CH_4 over this catalyst was only achieved at temperatures of 460 °C and above.

The catalytic activities of the PdO/CZB/Al_2O_3 catalysts were considerably higher than those of the Pt/CZB/Al_2O_3 catalysts, which is due to a difference in the chemical activity of oxygen on the surface of Pt and PdO particles. It has been reported that it is difficult to briefly activate the C–H bonds in CH_4 by a homolytic mechanism with the adsorbed oxygen on the Pt surface, whereas Pd^{2+} and O^{2-} ion pairs on the surface of fully oxidized PdO can easily activate the C–H bonds by a heterolytic mechanism [18]. The optimum amounts of Pt and PdO to impart the highest activities on the catalysts were approximately 7.3 wt% for Pt and 11.6 wt% for PdO. For catalysts containing larger amounts of Pt and PdO, the effectiveness of the dispersion was reduced by agglomeration and particle growth of the Pt and PdO particles. As a result, excess amounts of Pt and PdO have a negative effect on the catalytic activity. A similar result was obtained in the case of toluene combustion on the Pt/CeO_2–ZrO_2–Bi_2O_3/γ-Al_2O_3 catalysts, and agglomeration of platinum particles was confirmed in the transmission electron micrographs [26].

The dependence of catalyst formation on the calcination temperature was also examined. XRD patterns of the 11.6%PdO/CZB/Al_2O_3 catalysts prepared at 400, 500, and 600 °C are shown in Fig. 3. The full width at half maximum of the peaks assigned to the cubic fluorite structure is broader for lower the calcination temperature. The BET

Fig. 1 XRD patterns of the **a** Pt (5.3–15.2 wt%)/CZB/Al_2O_3 and **b** PdO (5.8–16.8 wt%)/CZB/Al_2O_3 catalysts prepared at 500 °C

Table 1 Composition and BET surface area of the catalysts prepared at 500 °C

Catalyst	Composition	BET surface area ($m^2 g^{-1}$)
Al_2O_3	γ-Al_2O_3	274
CZB/Al_2O_3	16 wt% $Ce_{0.64}Zr_{0.16}Bi_{0.20}O_{1.90}$/$\gamma$-$Al_2O_3$	192
5.3%Pt/CZB/Al_2O_3	5.3 wt% Pt/15 wt% $Ce_{0.63}Zr_{0.17}Bi_{0.20}O_{1.90}$/$\gamma$-$Al_2O_3$	177
7.3%Pt/CZB/Al_2O_3	7.3 wt% Pt/15 wt% $Ce_{0.64}Zr_{0.16}Bi_{0.20}O_{1.90}$/$\gamma$-$Al_2O_3$	173
9.9%Pt/CZB/Al_2O_3	9.9 wt% Pt/17 wt% $Ce_{0.63}Zr_{0.17}Bi_{0.20}O_{1.90}$/$\gamma$-$Al_2O_3$	166
15.2%Pt/CZB/Al_2O_3	15.2 wt% Pt/16 wt% $Ce_{0.64}Zr_{0.16}Bi_{0.20}O_{1.90}$/$\gamma$-$Al_2O_3$	158
5.8%PdO/CZB/Al_2O_3	5.8 wt% PdO/16 wt% $Ce_{0.62}Zr_{0.17}Bi_{0.21}O_{1.895}$/$\gamma$-$Al_2O_3$	178
8.0%PdO/CZB/Al_2O_3	8.0 wt% PdO/17 wt% $Ce_{0.62}Zr_{0.17}Bi_{0.21}O_{1.895}$/$\gamma$-$Al_2O_3$	176
11.6%PdO/CZB/Al_2O_3	11.6 wt% PdO/15 wt% $Ce_{0.62}Zr_{0.17}Bi_{0.21}O_{1.895}$/$\gamma$-$Al_2O_3$	176
16.8%PdO/CZB/Al_2O_3	16.8 wt% PdO/14 wt% $Ce_{0.63}Zr_{0.17}Bi_{0.20}O_{1.90}$/$\gamma$-$Al_2O_3$	169

Fig. 2 Temperature dependence of CH_4 oxidation over the **a** Pt (5.3–15.2 wt%)/CZB/Al_2O_3 and **b** PdO (5.8–16.8 wt%)/CZB/Al_2O_3 catalysts prepared at 500 °C

Fig. 3 XRD patterns of the 11.6%PdO/CZB/Al_2O_3 catalysts prepared at 400, 500, and 600 °C

specific surface areas of the 11.6%PdO/CZB/Al_2O_3 catalysts prepared at 400, 500, and 600 °C are summarized in Table 2. The specific surface area of the catalysts was significantly reduced with increasing calcination temperature.

The TEM images of the 11.6%PdO/CZB/Al_2O_3 catalysts prepared at 400 and 500 °C in Fig. 4 show that the primary particle size of the catalyst was about 10 nm, but they aggregated to form the secondary particles of which the size is between 2 and 5 μm. The dispersibility of PdO particles, which are recognized as dark, is higher in the sample prepared at 400 °C (Fig. 4a) than that prepared at 500 °C (Fig. 4b). This suggests that particle agglomeration is inhibited at lower calcination temperatures.
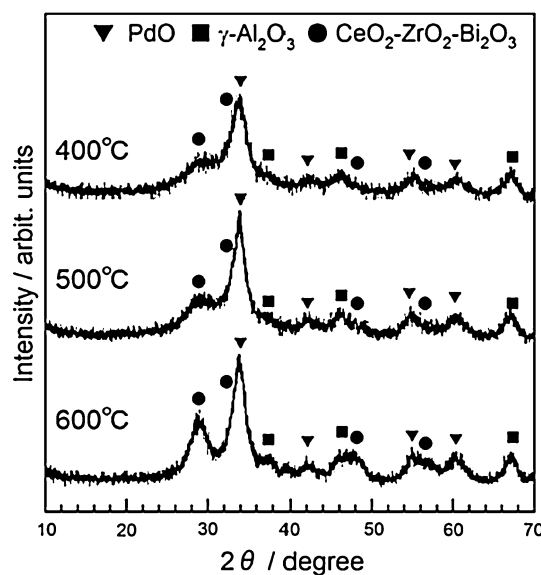
The temperature dependence of CH_4 oxidation on the 11.6%PdO/CZB/Al_2O_3 catalysts prepared at 400, 500, and 600 °C is shown in Fig. 5. Complete oxidation of CH_4 was realized at a temperature as low as 320 °C over the 11.6%PdO/CZB/Al_2O_3 catalyst prepared at the optimum calcination temperature of 400 °C. It was confirmed that the catalyst was stable and was not deactivated after being used for a week in a row: 100% conversion of CH_4 to CO_2 and steam was maintained even after being in the gas stream at 320 °C.

CH_4 combustion on the PdO-based catalysts follows a redox mechanism, and a variety of kinetic models for the

Table 2 BET surface area, specific reaction rate at 300 °C ($r_{300\ °C}$), and apparent activation energy (E_a) for total oxidation of CH_4 over the $11.6\%PdO/CZB/Al_2O_3$ catalysts prepared at 400, 500, and 600 °C

| Calcination temperature (°C)	BET surface area ($m^2\ g^{-1}$)	$r_{300\ °C}$ ($\mu mol\ s^{-1}\ g^{-1}$)	E_a ($kJ\ mol^{-1}$)
400	201	14.3	88
500	176	8.3	93
600	149	2.1	97

reaction rates of this reaction have been reported in the literature [28, 29]. In general, the reaction rate is strongly influenced by the partial pressure of CH_4, but is not significantly dependent on the oxygen partial pressure. Accordingly, the reaction becomes first order with respect to CH_4 and pseudo-zero-order with respect to oxygen [30, 31]. Although the general equation for the oxidation–reduction model is relatively complex, this equation can be reduced to a simple first-order kinetic model based on a power-law rate expression when an excess amount of oxygen is present, as follows:

$$r = kP_{CH_4} \tag{1}$$

where r is the reaction rate and k is the rate constant. The dependence of k on the temperature can be given by the Arrhenius equation:

$$k = A\exp(-E_a/RT) \tag{2}$$

where A is the pre-exponential factor, T is the reaction temperature in K, E_a is the apparent activation energy, and R is the gas constant. The CH_4 conversion is proportional to k; therefore, the apparent activation energy can be calculated from the slope of the Arrhenius plot, in which $\ln k$ is plotted against the reciprocal temperature. Figure 6 presents the resulting Arrhenius plots for the $11.6\%PdO/CZB/$
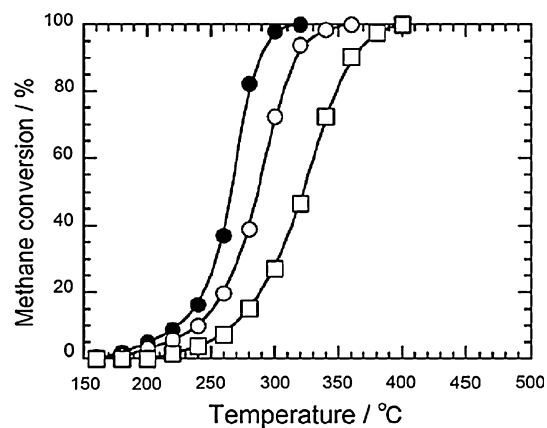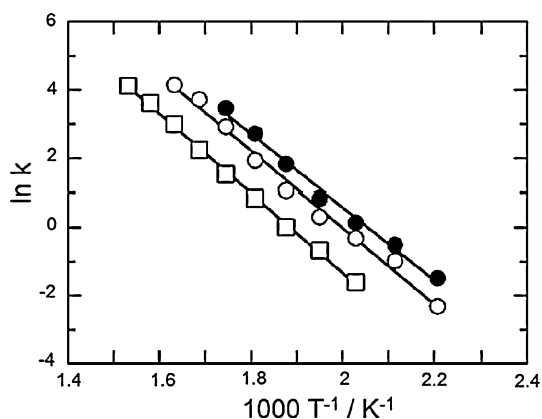

Fig. 5 Temperature dependence of CH_4 oxidation over the $11.6\%PdO/CZB/Al_2O_3$ catalysts prepared at 400 (*filled circle*), 500 (*open circle*), and 600 °C (*open square*)

Al_2O_3 catalysts prepared at 400, 500, and 600 °C and E_a for the catalysts are summarized in Table 2. The apparent activation energy for CH_4 conversion over the $11.6\%PdO/CZB/Al_2O_3$ catalyst prepared at 400 °C is 88 kJ mol^{-1}, which is in very good agreement with 86 kJ mol^{-1} for the $7.3\%PdO/Al_2O_3$ catalyst [31], 70–100 kJ mol^{-1} for the $5\%PdO/Al_2O_3$ catalysts [32], and 76 kJ mol^{-1} for the $8.5\%PdO/Al_2O_3$ catalyst [33]. Furthermore, the catalytic conversion activity in the flow reactor system was also evaluated by the specific reaction rate expressed per mass unit of the catalyst ($\mu mol\ s^{-1}\ g^{-1}$) at 300 °C. The $11.6\%PdO/CZB/Al_2O_3$ catalyst prepared at 400 °C has the highest reaction rate and lowest activation energy among the catalysts prepared at different temperatures, as summarized in Table 2, which is consistent with the catalytic activities shown in Fig. 5.
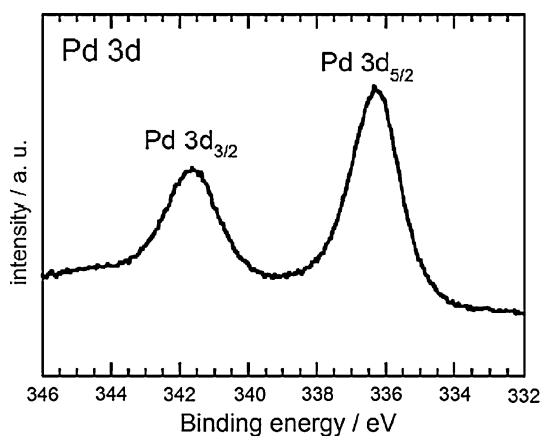
The chemical and electronic states of the $11.6\%PdO/CZB/Al_2O_3$ catalyst prepared at 400 °C were analyzed by
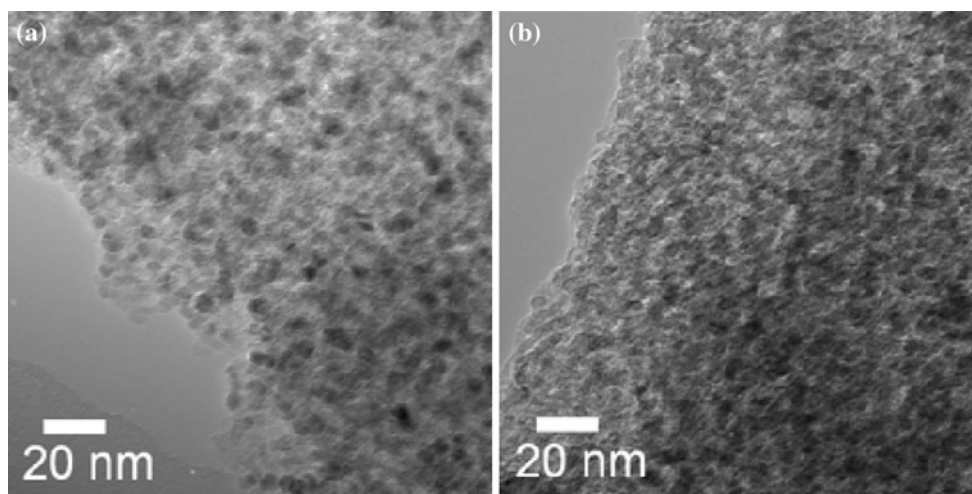
Fig. 4 TEM images of the $11.6\%PdO/CZB/Al_2O_3$ catalysts prepared at **a** 400 and **b** 500 °C

Fig. 6 Arrhenius plots for complete oxidation of CH_4 over the 11.6%PdO/CZB/Al$_2$O$_3$ catalysts prepared at 400 (*filled circle*), 500 (*open circle*), and 600 °C (*open square*)

Fig. 7 XPS of the Pd 3d core-levels of 11.6%PdO/CZB/Al$_2$O$_3$ catalysts prepared at 400 °C

XPS. The XPS of Pd 3d core-levels is shown in Fig. 7. The binding energies of Pd 3d$_{5/2}$ (336.3 eV) and Pd 3d$_{3/2}$ (341.7 eV) can be assigned to PdO [34], which is more active than metallic Pd for CH_4 oxidation [35]. The presence of PdO corresponds to the XRD pattern for the 11.6%PdO/CZB/Al$_2$O$_3$ catalyst prepared at 400 °C (Fig. 3). Oxidation of CH_4 over the PdO-based catalysts is accompanied by the reduction of PdO to metallic Pd, and then the metallic Pd is subsequently re-oxidized to PdO by reaction with adsorbed oxygen [36–38]. Furthermore, it has been reported that the addition of CeO_2 as a promoter to PdO/Al$_2$O$_3$ catalysts is effective to accelerate the re-oxidation of Pd to PdO due to the contribution of lattice oxygen from the CeO_2 bulk [39]. The Ce$_{0.64}$Zr$_{0.16}$Bi$_{0.20}$O$_{1.90}$ solid solution employed in this study is more active than CeO_2 to release oxygen from the bulk [22, 23], and accordingly, the re-oxidation of metallic Pd particles occurs more readily.

Conclusions

The complete oxidation of CH_4 was evaluated over Pt/CeO_2–ZrO_2–Bi_2O_3/γ-Al$_2$O$_3$ and PdO/CeO_2–ZrO_2–Bi_2O_3/γ-Al$_2$O$_3$ catalysts prepared in the presence of PVP. The catalytic activities of the PdO/CeO_2–ZrO_2–Bi_2O_3/γ-Al$_2$O$_3$ catalysts were higher than those of the Pt/CeO_2–ZrO_2–Bi_2O_3/γ-Al$_2$O$_3$ catalysts, due to the presence of fully oxidized PdO that can activate the C–H bonds in CH_4. Oxidation of CH_4 over the PdO/CeO_2–ZrO_2–Bi_2O_3/γ-Al$_2$O$_3$ catalyst was increased for lower catalyst calcination temperatures, whereby the activation energy was decreased and the reaction rate was increased. Lattice oxygen from the active CeO_2–ZrO_2–Bi_2O_3 bulk contributes to accelerate the re-oxidation of Pd into PdO for CH_4 oxidation. As a result, complete oxidation of CH_4 into CO_2 and steam was realized at temperatures as low as 320 °C over the 11.6 wt% PdO/15 wt% Ce$_{0.62}$Zr$_{0.17}$Bi$_{0.21}$O$_{1.895}$/γ-Al$_2$O$_3$ prepared at 400 °C.

References

1. Lampert JK, Kazi MS, Farrauto RJ (1997) Appl Catal B Environ 14:211
2. Thevenin PO, Menon PG, Järås SG (2003) Cattech 7:10
3. Lee JH, Trimm DL (1995) Fuel Process Technol 42:339
4. Choudhary TV, Banerjee S, Choudhary VR (2002) Appl Catal A Gen 234:1
5. Gélin P, Primet M (2002) Appl Catal B Environ 39:1
6. Ciuparu D, Lyubovsky MR, Altman E, Pfefferle LD, Daltye A (2002) Catal Rev Sci Eng 44:593
7. Gélin P, Urfels L, Primet M, Tena E (2003) Catal Today 83:45
8. Takeguchi T, Takeoh O, Aoyama S, Ueda J, Kikuchi R, Eguchi K (2003) Appl Catal A Gen 252:205
9. Arai H, Yamada T, Eguchi K, Seiyama T (1986) Appl Catal 26:265
10. Pengpanich S, Meeyoo V, Rirksomboon T, Bunyakiat K (2002) Appl Catal A Gen 234:221
11. Liotta LF, Carlo GD, Pantaleo G, Deganello G (2005) Catal Commun 6:329
12. Águila G, Gracia F, Cortés J, Araya P (2008) Appl Catal B Environ 77:325
13. Russo N, Palmisano P, Fino D (2009) Top Catal 52:2001
14. Oh SH, Mitchell PJ, Siewert RM (1991) J Catal 132:287
15. Cullis CF, Keene DE, Trimm DL (1970) J Catal 19:378
16. McCabe RW, McCready DF (1984) Chem Phys Lett 111:89
17. Lapinski MP, Silver RG, Ekerdt JG, McCabe RW (1987) J Catal 105:258

18. Burch R, Crittle DJ, Hayes MJ (1999) Catal Today 47:229
19. Imanaka N, Masui T, Minami K, Koyabu K (2005) Chem Mater 17:6511
20. Minami K, Masui T, Imanaka N, Dai L, Pacaud B (2006) J Alloys Compd 408–412:1132
21. Masui T, Minami K, Koyabu K, Imanaka N (2006) Catal Today 117:187
22. Imanaka N, Masui T, Koyabu K, Minami K, Egawa T (2007) Adv Mater 19:1608
23. Masui T, Koyabu K, Minami K, Egawa T, Imanaka N (2007) J Phys Chem C 111:13892
24. Imanaka N, Masui T, Terada A, Imadzu H (2008) Chem Lett 37:42
25. Imanaka N, Masui T (2009) Chem Rec 9:40
26. Masui T, Imadzu H, Matsuyama N, Imanaka N (2010) J Hazard Mater 176:1106
27. Yasuda K, Nobu M, Masui T, Imanaka N (2010) Mater Res Bull 45:1278
28. Hayes RE, Kolaczkowski ST, Li PKC, Awdry S (2001) Chem Eng Sci 56:4815
29. Hurtado P, Ordóñez S, Sastre H, Díez FV (2004) Appl Catal B Environ 51:229
30. Cullis CF, Willatt BM (1983) J Catal 83:267
31. Van Giezen JC, Van den Berg FR, Kleinen JL, Van Dillen AJ, Geus JW (1999) Catal Today 47:287
32. Baldwin TR, Burch R (1990) Appl Catal 66:337
33. Ribeiro FH, Chow M, Dalla Betta RA (1994) J Catal 146:537
34. Pillo T, Zimmermann R, Steiner P, Hüfner S (1997) J Phys Condens Matter 9:3987
35. Farrauto RJ, Hobson MC, Kennelly T, Waterman EM (1992) Appl Catal A Gen 81:227
36. McCarty JG (1995) Catal Today 26:283
37. Datye AK, Bravo J, Nelson TR, Atanasova P, Lyubovsky M, Pfefferle L (2000) Appl Catal A Gen 198:179
38. Thevenin PO, Pocoroba E, Pettersson LJ, Karhu H, Väyrynen IJ, Järås SG (2002) J Catal 207:139
39. Thevenin PO, Alcalde A, Pettersson LJ, Järås SG, Fierro JLG (2003) J Catal 215:78